A Model-Based Precipitation Study of Copper-Based Catalysts

Martin A. J. Hartig and Wolfgang Peukert
Dept. of Particle Technology, Friedrich-Alexander University, Cauerstraße 4, Erlangen 91058, Germany

Nikolas Jacobsen
Clariant Produkte (Deutschland) GmbH, Waldheimer Straße 13, Bruckmühl 83052, Germany

Alexander Leuthold
CeramTec GmbH, Luitpoldstraße 15, Lauf 91207, Germany

DOI 10.1002/aic.14810
Published online April 13, 2015 in Wiley Online Library (wileyonlinelibrary.com)

Numerical methods of particle technology are used to model the formation of catalyst precursors with the purpose to control disperse properties. A multicomponent and multiphase population balance model is applied to the precipitation of catalyst precursors in a T-mixer. Copper precursors are chosen to be investigated in detail as a basis for catalysts with a broad range of applications such as in methanol synthesis, water-gas shift and hydrogenation reactions. The simulations results could be validated by ex situ measurements such as the pH of the suspension, the solid dry weight of the precipitate, and the yield. Simulations show that dissociation reactions of copper and carbonate species in water control significantly the formation of Georgeite. Consumption of the copper component by solid formation can be controlled in a range of 20–100% by the adjustment of the pH of the copper nitrate reactant solution. © 2015 American Institute of Chemical Engineers *AIChE J*, 61: 2104–2116, 2015
Keywords: catalyst preparation, precursor chemistry, methanol synthesis, population balance, mixing

Introduction

According to Deutschmann et al. "precipitation and coprecipitation are the most frequently applied methods for the preparation of unsupported catalysts."[1] The resulting mixed metal oxides are applied in broad range of industrial processes.[1] Various mixed metal oxide catalysts contain copper as the basic active component and are produced by coprecipitation: $Cu/ZnO/Al_2O_3$ for the large-scale synthesis of methanol[2] and the hydrogenation of fatty acid esters,[3] Cu/Mn_2O_4 for the oxidation of CO[4], $Cu/Co/MoO_x$ catalysts for the selective conversion of synthesis gas to ethanol and higher alcohols,[5] Cu- and Ag-modified cerium oxide catalysts for methane oxidation,[6] and Cu- and Ni-containing cerium oxide catalysts for the low temperature water-gas shift reaction.[7] The production of these catalysts follows the process chain: precipitation of metal salts, aging of the precipitate, washing and filtration, drying, shaping, and activation.[1] This work focuses on the investigation of the first step, that is, the precipitation of the copper precursors. The objective is to gain a deeper understanding of the particle formation of copper-based catalysts by simulations and experiments.

Recently, alternative reactant solutions were used for the preparation of methanol catalyst precursors. For instance, potassium carbonate, ammonium carbonate, or sodium hydroxide were used as bases.[8,9] Simson et al. found that catalysts which are prepared with ammonium carbonate have a similar activity as conventional prepared catalysts.[9] Copper and zinc formates[10] and magnesium nitrates[11] are discussed as alternative metal salts to copper nitrate. Rosasite $(Cu_{1-x}Zn_x)_2(OH)_2CO_3$ with a high substitution of copper by zinc is favored as active methanol catalyst precursor phase.[12] The zinc content is limited to 30% in case of using copper and zinc nitrate as reactants.[12] In Cu, Mg minerals such as McGuinessite $(Cu,Mg)_2(OH)_2CO_3$, a magnesium content of 50% and above was found. Hence, Cu, Mg precursors are promising catalyst materials by the higher substitution of copper than in case of Cu, Zn minerals.[11] In practice, many different compositions have to be tested for the development and optimization of a new catalyst formulation. Experiments and characterizations of the catalyst products must also be performed along the process chain for each new formulation. Preparation conditions, such as the adjustment of the pH during precipitation, may vary considerably from the standard routine. The transfer of know-how of the thoroughly experimentally studied standard routine toward alternative routes is demanding or even impossible. Hence, there is a huge demand of a model which especially can take into account the dissociation reactions of different metal salts and bases in aqueous media.

In this work, it is shown that the multicomponent and multiphase model of Hartig et al. is capable to satisfy the demand.[13] It is applied here to the precipitation of Georgeite as copper catalyst precursor phase. Numerical studies are performed purposefully and are validated experimentally. By this, important insights into the complex catalyst formation

Additional Supporting Information may be found in the online version of this article.

Correspondence concerning this article should be addressed to W. Peukert at wolfgang.peukert@fau.de.

mechanisms are given. Relevant process parameters for the production of copper catalyst precursors are derived. In particular, the pH of reactant solutions could be identified as process parameter to significantly control the conversion of the copper component.

Experimental

Catalyst preparation in a T-mixer

A T-mixer is used for the semibatch precipitation of the catalyst precursors. The device was used before in several studies to investigate particularly the influence of mixing on precipitation. Precipitation systems under investigation were barium sulfate, zinc oxide, lead (II) sulfide, or cadmium sulfide.[14,15] Micromixers were used before to prepare methanol catalysts.[16,17] However, the focus of these publications were on the continuous production of catalysts. In this work, the reactant solutions are pumped through the T-mixer by an oscillation free syringe pump with a flow rate between 0.2 and 12 mL/s. The T-mixer module consists of two inlets. In case of catalyst preparation the first inlet is used for the supply of the copper nitrate solution and the second inlet is used for the supply of the sodium carbonate solution. The outlet is connected directly to a Schott flask in which the suspension is collected. For each precipitation experiment, 50 mL of each of the two reactant solutions is pumped through the T-mixer.

The mixing zone inside the T-mixer module has a length of 10 mm and a rectangular cross section of 1 mm. By pressure loss calibration, a pressure drop coefficient of 1.65 could be found. The pressure drop is used to approximate the mean specific power input in the global mixing model of Schwarzer and Peukert.[18] A dead volume of the feeding pipes was detected by calibration of the T-mixer device. The actual reactor volume is 88.5 mL (V_{reactor}). The remaining reactant solutions in the feed pipes are removed after each precipitation by rinsing the T-mixer with 200-mL water.[13]

Reactant solutions

The reactant solutions are prepared by dissolution of salts in bidistilled water. For the copper nitrate reactant solution, copper(II) nitrate trihydrate $Cu(NO_3)_2{\cdot}3H_2O$ (purity $\geq$ 99%, Acros Organics, Germany) is used. Sodium carbonate Na_2CO_3 (purity $\geq$ 99.8%, water free, Roth, Germany) is used to prepare the base solution. Commonly the pH of precipitation in stirred vessels is controlled by the flow rate of the sodium carbonate or copper nitrate solution. In case of using the T-mixer the flow rates are equal. Another option to adjust the pH is the addition of nitric acid to the copper nitrate solution before precipitation. The volume of nitric acid to adjust the pH to a value of pH_0 is calculated by equation

$$V_{\text{HNO}_3} = \frac{10^{-\text{pH}_0}[\text{M}] \cdot V_{\text{H}_2\text{O}} \cdot \text{M}_{\text{HNO}_3}}{\rho_{\text{HNO}_3} - 10^{-\text{pH}_0}[\text{M}] \cdot \text{M}_{\text{HNO}_3}} \tag{1}$$

assuming complete dissociation of nitric acid in water. According to Eq. 1, the addition of 0.9 mL of concentrated nitric acid ($M(HNO_3) = 63.01$ g/mol, $\rho_{HNO_3} = 1400$ kg/m^3) is necessary to adjust a 200-mL reactant solution to pH one ($pH_0 = 1$). The concentration of nitric acid with respect to the whole reactant solution is 0.095 M.

Ex situ *characterization of suspension and precipitate*

The pH of the suspension is measured over the first 10 s. Immediately after measuring the pH, the suspension is transferred to the filter device and filtrated using a cellulose acetate filter paper with a pore size of 0.2 μm purchased from Sartorius. The filter cake is washed with 200-mL bidistilled water. To prepare samples for scanning electron microscopy (SEM), 0.01 g of the filter cake was resuspended in 5-mL bidistilled water. One drop of the suspension is dried on a silicon wafer. To obtain a dry powder, the washed filter cake is dried overnight in an oven at 50°C to obtain the solid dry weight.

For microscopic investigations, an SEM Ultra 55 (Zeiss) is used with a SE2-detector with an accelerating voltage of 2 kV. The precipitate is characterized by inductively coupled plasma atomic emission spectroscopy (ICP-AES, Perkin Elmer Optima 8300). Nitric acid is used as a masking agent to prepare the solutions for ICP-AES measurements. The devices Euro EA 3000 (Euro Vector) and EA 1108 (Carlo-Erba) are used for elemental analysis to obtain the H, C, and N content of the precipitates. Additionally, the Kjeldahl method is used to investigate the N content of the precipitates.

Model

A multicomponent and multiphase model is presented in the work of Hartig et al., which is applied here to the Georgeite formation in a T-mixer.[13] In the following, we summarize the model briefly. The dissociation reactions of species in aqueous media are considered by Eq. 2

$$c_{\text{tot},p} - \sum_{j=1}^{N_j} \alpha_{j,p} K_j^C \prod_{p=1}^{N_p} c_p^{\alpha_{j,p}} = 0 \tag{2}$$

which contains the total concentration of components $c_{\text{tot},p}$, coefficient parameter α_{jp}, equilibrium constants K_j^C, and concentration of components c_p. The total concentration of each component distributes in concentrations of species which is expressed as a summation term in Eq. 2. Each concentration of species is calculated in turn by the mass law, which is expressed in Eq. 2 by the product term of components' concentrations. Equation 2 is a nonlinear system of equations which scales with the number of components N_p and species N_j and is solved for the concentrations of components by the Newton–Raphson method. The concentrations of components can be used to calculate the concentrations of species and in turn the supersaturations in each time step of simulation. Activities are calculated from the concentrations extended Debye–Hückel activity correction according to Davies.

Hartig et al.[13] presented an overall multidimensional population balance of primary particles containing multiple solid phases and simplified it to

$$\frac{\partial n_i(x,t)}{\partial t} = -\frac{\partial}{\partial x}[G_i(x) \cdot n_i(x,t)] + B_{\text{hom},i} \cdot n_{\text{nuclei,hom}} + B_{\text{sec},i} \cdot A_i \cdot n_{\text{nuclei,sec}} + \sum_{j=1,\ j\neq i}^{N_i} B_{\text{het},ij} \cdot A_j \cdot n_{\text{nuclei,het}} \tag{3}$$

assuming separate formation of primary particles of different solid compositions and plug flow conditions in the mixing zone in a T-mixer with 1-D spatial resolution. For each solid phase i in the precipitation system, one population balance Eq. 3 can be setup. Equation 3 considers particle formation by growth homogeneous, secondary and heterogeneous nucleation. One can find the corresponding terms in the

right-hand side of Eq. 3. In each nucleation term, the nuclei size distribution and nucleation rate have to be considered. According to Mersmann, nucleation can be subdivided into primary and secondary nucleation.[19] The primary nucleation can be again subdivided into homogeneous and heterogeneous nucleation. The latter mentioned mechanism occurs at surfaces of different kinds of particles, the reactor wall or at gas-liquid interfaces. In Eq. 3, only the nucleation on the surfaces of particles of different solid phases is considered. The precipitation takes place in a T-mixer without contact to the surrounding atmosphere. Hence, due to the small surface area of the reactor relative to the particle surfaces and due missing gas bubbles, only heterogeneous nucleation at the surface of particles is considered. By the definition of Mersmann, secondary nucleation is associated with nuclei, which are created by mechanical impact such as fracture of needles by impacting on the stirrer.[19] This kind of nucleation is neglected because nanoparticles are formed which cannot be stressed mechanically inside the T-mixer. However, in this work, the secondary nucleation refers to the formation of nuclei on the surface of already formed particles of the very same solid phase.[20] Mersmann calls this phenomena surface nucleation and derived a rate expression, which is used in this work.[19]

In this work, it is assumed that the primary particles consist of only one solid phase Georgeite ($N_i = 1$, $i =$ Georgeite). The diameter of spherical primary particles of Georgeite is used as only internal coordinate. In this case, Eq. 3 can be simplified to one 1-D population balance[13]

$$\frac{\partial n(x,t)}{\partial t} = -\frac{\partial}{\partial x}[G(x)\cdot n(x)] + B_{\text{hom}}\cdot n_{\text{nuclei,hom}}(x) + \underbrace{B_{\text{sec}}(\gamma_{\text{sec}})\cdot A}_{B_{\text{eff}}}\cdot n_{\text{nuclei,sec}}(x). \tag{4}$$

The index of Georgeite ($i =$ Georgeite) is not shown in Eq. 4 for the purpose of readability. The term on the left-hand side of Eq. 4 describes the temporal change of the Georgeite particle size distribution by growth (first term, right-hand side of Eq. 4), homogeneous (second term, right-hand side of Eq. 4), and secondary (third term, right-hand side of Eq. 4) nucleation. Heterogeneous nucleation is not considered in Eq. 4 because of the aforementioned reasons and as only one solid phase is formed. Equation 4 contains the nuclei size distributions n_{nuclei} of homogeneous (index "hom") and secondary nucleation (index "sec"). For nucleation expressions from classical nucleation theory were taken to estimate the rates and the critical nuclei sizes. Hartig et al. derived a multicomponent growth rate G, which is based on diffusion-limited growth of each single component from the solution.[13] Why diffusion-limited growth has been assumed for Georgeite formation is explained in the Disperse Properties of Precursors section. Hence, components' concentrations from Eq. 2 determine the growth rate. The homogeneous and secondary nucleation rates are calculated using species' activities from Eq. 2 and material parameters. One important material parameter is the interfacial energy γ, which is corrected by the adhesion factor β_{sec} in case of secondary nucleation[13,20]

$$\gamma_{\text{sec}} = \frac{\gamma}{k_{\text{A}}}\cdot(k_{\text{A}} - \beta_{\text{sec}}) \tag{5}$$

The shape factor k_{A} of a sphere is used in Eq. 5. The affinity of secondary nuclei toward the particle surface and hence, the secondary nucleation rate increases with increasing β_{sec} The range of β_{sec} is between 0 and 2. The total surface area of particles A, which is considered in the term of secondary nucleation in Eq. 4, provides nucleation sites for secondary nucleation. The product of secondary nucleation rate B_{sec} and total surface area A is summarized as effective secondary nucleation rate B_{eff}.

Equation 6 balances the temporal change of components' total concentrations in the solution

$$\frac{dc_{\text{tot},p}}{dt} = \mathcal{M}_p - \beta_p \dot{c}_{\text{solid}} \tag{6}$$

by mixing and formation of one solid Georgeite. The original balance equation can be found in the publication of Hartig et al.[13] The particle formation leads to a decrease of components' concentrations and is expressed as the product of coefficient parameter β_p and change of solid concentration $\dot{c}_{\text{solid}}$. The change of solid concentration $\dot{c}_{\text{solid}}$ can be calculated in each time step of simulation by the third moment of the particle size distribution in Eq. 4. β_{p} reflects the stoichiometry of the solids in terms of components. Mixing leads to an increase of total components' concentrations in the mixing zone. The mixing term $\mathcal{M}_p$ in Eq. 6 can be derived from the global mixing model.[13]

Equations 2, 4, and 6 are strongly coupled. An algorithm to solve these equations is presented in the publication of Hartig et al.[13] The direct quadrature method of moments direct quadrature method of moments (DQMOM) is used to solve the population balance equation, Eq. 4. The resulting set of ordinary differential equations including Eq. 6 is solved in the Matlab software Version R2011b using the integrated *ode23* solver, which is based on the implementation of an explicit Runge-Kutta (2,3) pair of Bogacki and Shampine.[21] The solution of the nonlinear system of equations, Eq. 2 is gained in each time step by an in Matlab own implemented solver, which is based on the Newton–Raphson method.[22] Information about coefficient parameters, details of particle formation kinetics and material parameters can be taken from the publication.[13]

Results and Discussion

Influence of preparation parameters on the precipitation in the T-mixer

The discussion of preparation parameters, in this section, leads to a choice of reference conditions for the experimental validation. The reference conditions are summarized in the next section. The postprocessing procedure was adopted from Bems et al. in which bidistilled water at ambient temperature is used for filtration.[2] The postprocessing parameters are chosen to minimize any influence of postprocessing on the characterization of the precipitate.

Widespread structures with a plate-like morphology could be observed in SEM images, if the unwashed suspension was dried on the silicon wafer. This morphology is known for the crystalline ageing products of catalyst preparation.[23] During drying, remaining free ions in the aqueous phase crystallize on the silicon wafer. However, an excessive use of wash water can lead to an under saturated suspension and to the dissolution of the precipitate. Hence, we used only 200-mL bidistilled water as wash water. Since the measured pH did not change significantly (pH difference in the range of 0.5) by washing and filtration, we can assume that no ions were released into the solution because the latter would lead to a change of the pH. Hence, the effect of the washing

Table 1. Reference Conditions of Precipitation

	Not acidified/ without addition of nitric acid	Acidified/with addition of nitric acid
Na_2CO_3 conc. (M[a])	0.13	
$Cu(NO_3)_2$ conc. (M)	0.1	
HNO_3 conc. (M)	0.0	0.095[b]
Flow rate (mL/s)	3	
Temperature (°C)	Room temperature 25 °C	

[a]The unit kmol/m^3 is abbreviated in the manuscript as M.
[b]Declared as 0.1 M HNO_3 in the legends in this manuscript.

procedure on the disperse properties of the precipitate can be neglected. The filtration is performed within 20 min like in the published postprocessing procedure of Zander et al. to obtain "unaged" precursors.[8]

The oven temperature to dry the precipitate overnight was set to a low temperature of 50°C. Georgeite $Cu_2CO_3(OH)_2$ contains carbonate and hydroxides, which can degas as carbon dioxide or water during heat treatment.[2] A long-term drying experiment for 200 h at 50°C did not lead to any additional loss mass of the overnight dried solid. Hence, the applied drying procedure here does not change the composition of the solid.

The concentrations of copper nitrate and sodium carbonate reactant solutions have an impact on the postprocessing. At low concentrations (< 0.05 M), the amount of solid in suspension is so low that the mass of dried filter cake is in the range of the loss of mass by postprocessing. During filtration small amounts of the precipitate can stick to the wall of the filtration device. Furthermore, small amounts of remains cannot be excluded in the wash water. Hence, this range of operation is unsuitable for the preparation. At too high concentrations (> 0.2 M), the viscosity of suspension is very high. The filtration of the viscous suspension is not feasible until 20 min.

The restriction of the model assumptions in Model section comes mainly from the used activity correction. The extended Debye–Hückel activity model can be used up to an ionic strength of 0.7 M.[24] Hartig et al. showed that for an acidified copper nitrate reactant solution, the measured and calculated pH agree well up to an ionic strength of 0.33 M.[13] At copper nitrate reactant concentrations below 0.01 M, the partial dissolution of carbon dioxide in the solution from the atmosphere has to be considered. In this case also copper carbonate species which are reported in Hartig et al. should be included in Eq. 2.[13] Additionally, a defined atmosphere during precipitation is needed in the lab.

Reference conditions of preparation

The reference concentration of the copper nitrate reactant solution is chosen to be 0.1 M. This concentration is well above the concentration range in which atmospheric carbon dioxide would influence the precipitation. Additionally, the filtration can be performed within 20 min. This ensures that the postprocessing has minor influence of the characterization of the precipitate.[8]

The sodium carbonate reactant concentration is chosen arbitrarily to be 0.13 M. The influence of mixing on precipitation was already discussed in the publication of Hartig et al.[13] The focus of this study is to investigate the influence of reactant concentration on the precipitation. The flow rate is adjusted to 3 mL/s (2.2×10^3 W/kg) in which no influence of mixing could be observed.[13] Hence, the influence of reactant concentrations on precipitation can be investigated apart from the mixing influence. The pH of the copper nitrate reactant solution can be adjusted as explained in the Experimental section to a pH of approximately of 1. Accordingly, the reference conditions can be subdivided into precipitation with and without addition of nitric acid. The precipitation experiments were performed at room temperature. A temperature increase caused by particle formation and dissociation reactions was not observed in experiments. Hence, material parameters at 25 °C are used in the simulations. The reference conditions are summarized in Table 1.

Disperse properties of precursors

The investigation and discussion of the disperse properties of prepared catalyst precursors are essential for comparison of simulations and experiments in the following sections. The phase composition of copper catalyst precursors was already investigated in several studies.[8,25–27] However, the preparation conditions such as reactants or mixing devices vary significantly in comparison to this work. Hence, disperse properties of copper catalyst precursors prepared by the procedure in the last section are studied here in detail. The precipitated amorphous precursors cannot by investigated by X ray powder diffraction in contrast to the crystalline-aged catalyst precursors.[12,28,29] UV–visible spectra, titrations, and ICP-AES are used as complementary methods to study the precipitates' composition. It can be given in fractions $X_{i,p}$ of components or elements p in respect to solid i

$$X_{i,p} = \frac{\beta_{i,p} \cdot M_p}{\sum_{p'=1}^{N_p} \left(\beta_{i,p'} M_{p'}\right)} \tag{7}$$

The weight-based content $X_{i,p}$ can be calculated by dividing the molar mass of the component by the molar mass of the solid. The stoichiometry of the component within the solid has to be considered in Eq. 7 by $\beta_{i,p}$. The solid can be decomposed into components. Hence, the molar mass of the solid can be calculated by the summation of the components' molar masses considering their stoichiometry $\beta_{i,p}$ in the denominator of Eq. 7.

In Table 2, the phase composition in terms of copper $X_{i,\mathrm{Cu}}$ is listed for different relevant minerals. The minerals are reported in literature or can be derived from the components of the used reactant solutions.

The phase composition varies in a wide range from approximately 28% up to 80%. This allows us to identify the precipitate as a mineral by the copper content. Therefore, the measured content of copper, hydrogen H, carbon C, and nitrogen N of acidified and not acidified reference samples are summarized in Figures 1 and 2. The copper content by ICP measurements is in both samples about 55%. In Table

Table 2. Content of Relevant Copper Minerals

Mineral Name i	Chemical formula	Copper (wt %) $X_{i,\mathrm{Cu}}$
Tenorite[a]	CuO	79.9
–[a]	$Cu(OH)_2$	65.1
Gerhardtite[a]	$Cu_2(OH)_3(NO_3)$	53.0
Malachite[a]/Georgeite[b]	$Cu_2(OH)_2(CO_3)$	57.5
–[c]	$Na_2Cu(CO_3)_2$	27.7

[a]Ref. 2.
[b]Ref. 25.
[c]Ref. 17.

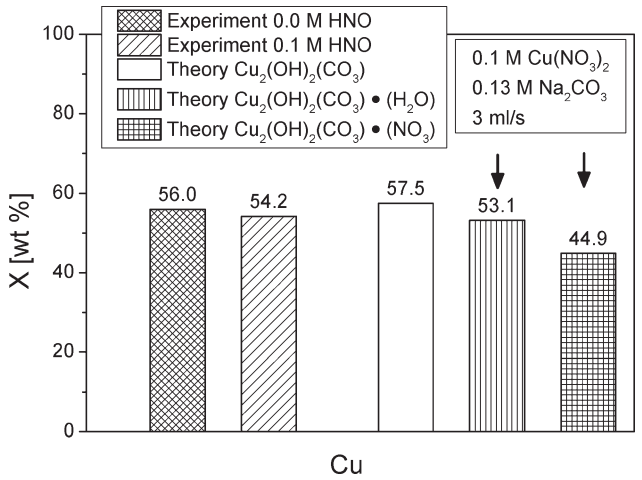

Figure 1. Copper content of acidified and not acidified precipitates in terms of weight fractions of elements (experiment) in comparison to the solid composition of malachite (theory) with or without inclusion of water or nitrate.

2, Georgeite and Gerhardtite are reported in the relevant copper content range of 50%–60%. The nitrogen content of both reference samples was measured with the Kjeldahl method and elemental analysis. The low content of the Kjeldahl method (acidified 1.1%, not acidified 1.8%) and elemental analysis (acidified 0.3%, not acidified 0.4%) supports the formation of Georgeite, which has no nitrate component incorporated in the crystal lattice. In case of Gerhardtite, the nitrogen content is expected to be much higher. In a further step, the composition calculated from Georgeite (theory) is compared with measured concentrations in Figures 1 and 2.

The measured phase composition is in good agreement with the phase composition of Georgeite $Cu_2(OH)_2(CO_3)$. The copper content deviates maximally by 3.2% (Figure 1) and the contents of elemental analysis deviate maximally by 1.2% (Figure 2). The deviation can be explained by remains on the surface or in cavities of the amorphous solid. Drying under mild conditions as explained in the Experimental section can lead to water residues in the solid. Nitrate from the copper nitrate reactant solution which is not consumed by solid formation should be removed by the washing procedure. However, the complete removal by the washing water cannot be expected. Elemental analysis is commonly used for crystalline structures. Hence, there is an additional uncertainty due to the inhomogeneous combustion of the amorphous precursors. The changes of the calculated contents of Georgeite by incorporation of water and nitrate are indicated by arrows in Figures 1 and 2. Two potential extreme cases of theoretical crystal structures with incorporation of water $Cu_2(OH)_2(CO_3)\cdot(H_2O)$ and incorporation of nitrate $Cu_2(OH)_2(CO_3)\cdot(NO_3)$ are considered. The ratio of solid toward the incorporated molecule is in both cases 1:1. This high ratio would cause a charging of the precipitate in case of nitrate contamination. The ratios are used to demonstrate the trend of change of the content. In reality, nitrate impurities will cause lower ratios so that the electron neutrality is nearly fulfilled. The copper content (Figure 1) and carbon content (Figure 2) decreases in both cases by incorporation of water or nitrate. The hydrogen content (Figure 2) increases in case of water residues. The nitrogen content (Figure 2) increases by incorporation of nitrate, which can explain the content of nitrogen by elemental analysis and the Kjeldahl method. Hence, the precipitate at reference preparation conditions can be identified as Georgeite by theoretical and experimental analysis of the phase composition considering small amounts of water and nitrate. Further measurements (see Supporting Information) in a wide range of preparation conditions ($Cu(NO_3)_2$ reactant concentration 0.05–0.13 M, Na_2CO_3 reactant concentration 0.075–0.15 M; 3–9 mL/s flow rate) show a mean copper content of 54.5% with a standard deviation of 2.6%, which is in the same range as at reference conditions. By this, Georgeite is expected to form in all preparation conditions in this work. Hartig et al. showed by simulations that the formation of Georgeite is favored in comparison to the formation of Gerhardtite or copper hydroxide.[13] The formation of Georgeite could be confirmed here by investigations of the solid composition.

The morphology is another important disperse property of the precipitate. In Figure 3, an exemplary SEM image is shown for the precipitation under reference conditions in Table 1 with addition of nitric acid.

Closely connected spherical particles can be recognized in Figure 3. The agglomerates consist of primary particles in the size range of nanometers. In the sample, two size fractions can be observed. By image analysis of Figure 3, a fine fraction below 50 nm and a larger-sized fraction which consist of primary particles with a diameter of approximately 50–180 nm can be observed. The fine particle fraction lies on the surface of the larger spherical particles and on the silicon wafer.

Spherical primary particles can be seen in Figure 3. These rounded particles may be formed during diffusion-controlled growth since the building units are integrated into the particles more or less wherever they hit the surface.[30] Growth units which are slowly integrated into the surface of the particles conserve the crystalline structure from the very beginning of particle formation resulting in more or less crystal-type morphologies. Possible integration sites of integration-controlled growth on the particle surface are kink sites, step, and screw-dislocations. These are not observed in Figure 3. Mersmann reports that integration-controlled occurs at low supersaturations and transits to transport-controlled growth

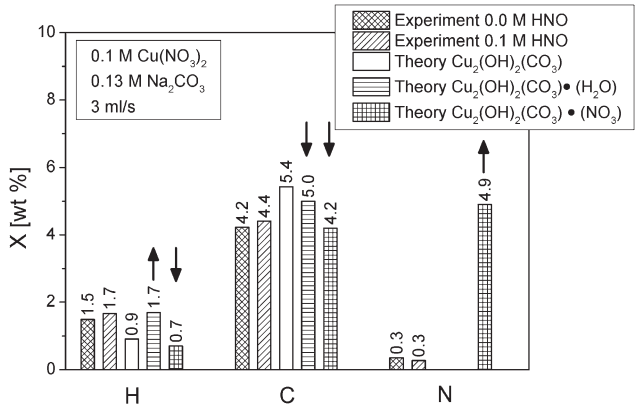

Figure 2. H, C, and N content of acidified and not acidified precipitates in terms of weight fractions of elements (experiment) in comparison to the solid composition of malachite (theory) with or without inclusion of water or nitrate.

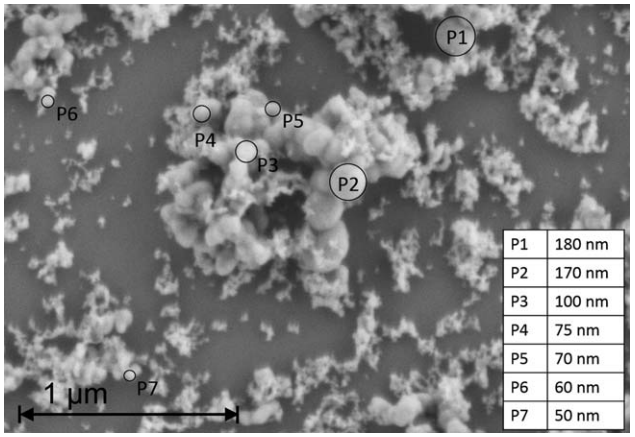

Figure 3. Scanning electron microscopy image of precipitates at reference conditions with addition of nitric acid to the copper nitrate reactant solution.

with increasing supersaturation.[19] The relatively high reactant concentrations, in case of catalyst precursor preparation supports diffusion controlled growth. On this basis, we assume diffusion-controlled growth in our simulations of copper catalyst precursor formation.

From simulations predicted, mean sizes of the primary particles are shown in Figure 4. The preparation conditions were varied in the simulations according to our experiments.

One simulation is run for each set of preparation conditions under assumptions and conditions defined in the Model section. The mean particle sizes are taken from simulations at arbitrary time t_{end} of 1 s in which the mean particle size has converged. The mean sizes in Figure 4 are in a range between 1 and 36 nm. In Figure 4, it can be seen that small mean particle sizes are predicted at low reactant concentrations and with the use of nitric acid. Under this conditions, the extent of secondary nucleation increases in our simulations. Further details are given in the next section. Simulations of Hartig et al. could show that with increasing extent of secondary nucleation, the mean particle size decreases significantly and is in the order of the critical nuclei size.[13] These nuclei have the size of the critical nuclei size and are assumed in the model to form as separate primary particles. Agglomeration and growth by secondary nucleation is not yet considered in the population balance Eq. 3. Hence, the mean particle sizes in the simulations are low by the creation of secondary nuclei. A further experimental estimation of the disperse properties of catalyst precursors could help us to validate our predicted particle sizes in future. However, the focus of this work is on the influence of preparation parameters on macroscopic results such as pH of suspension or solid concentration. They are used to compare simulations and experiments in the next section.

Global parameters of catalyst formation

The experimental solid dry weight is shown in Figure 5 for different reactant concentrations with and without the addition of nitric acid. The small error bars of the solid dry weight in Figure 5 are an indicator for the good reproducibility of the experiments using a T-mixer. An exception can be seen at high copper nitrate reactant concentrations and usage of nitric acid.

The solid dry weight increases with and without addition of nitric acid with the increase of reactant concentrations. The solid dry weight ranges from approximately 0.2 to 0.6 g. The solid mass using acidified preparation conditions is always lower than in the case of not acidified preparation conditions. The differences occur mainly at high copper nitrate concentrations or lower sodium carbonate concentrations. These differences can be explained by the dissociation reactions in aqueous media at varying reactant concentrations. This phenomenon is discussed in the last section based on simulation results. In the first instance, the reactant concentration can be used as an estimate for the maximal possible solid weight

$$m_{\text{solid,maximal}} = \min_{\beta_p>0} \left(\frac{c_{\text{tot},p}(t=0)}{2 \cdot \beta_p} \right) \times M_{\text{solid}} \times V_{\text{reactor}} \quad (8)$$

The minimal component's concentration (first factor in Eq. 8) limits the maximal solid concentration. In Eq. 8, a dilution factor of 2 is used to correct the total components' concentrations from the reactant concentration. The T-mixer is operated with equal feed flow rates. Hence, only half of the total components' concentrations can be used for particle formation by dilution of reactant solutions. Additionally, the stoichiometry of the solid phase β_p in terms of components has to be considered to find the minimal concentration. In case of Georgeite, 2 mol of copper is used for the formation 1 mol solid. Hence, from, for example, 0.1 M $c_{\text{tot,Cu}^{2+}}(t=0)$, whereas carbonate is in excess, 0.05 M c_{solid} can be formed. The reactor volume and the molar mass is used in Eq. 8 to convert the concentration into the total mass. The estimation of solid weight by components' concentrations is indicated by a solid line in Figure 5. The estimation holds only for low copper nitrate or high sodium carbonate reactant concentrations.

To improve the quality of estimation, the solid weight is taken from simulations. To compare experiment with simulation, the solid weight is calculated

$$m_{\text{solid}} = c_{\text{solid}}(t=t_{\text{end}}) \times V_{\text{reactor}} \times M_{\text{solid}} \quad (9)$$

using the simulated solid concentration c_{solid}, the reactor volume V_{reactor} and the molar mass of Georgeite M_{solid}. The solid concentrations are taken from simulations at arbitrary time t_{end} of 1 s in which the solid concentration has converged.

The pH of the suspension and the solid weight are summarized in Figure 6 for the precipitation with and without addition of nitric acid. Figure 6 includes the variation of the copper nitrate reactant concentration $c_{\text{reactant.Cu(NO}_3)_2}$ from reference conditions (Table 1). The experimental pH varies in a wide range from approximately 10 to 5.5 by variation of $c_{\text{reactant.Cu(NO}_3)_2}$ without use of nitric acid (Figure 6a). Also the experimental solid weight varies significantly between 0.2 and 0.6 g in Figure 6b. The pH decrease can be explained by the addition of acidic copper nitrate solution to sodium carbonate. The formation of Georgeite is accompanied by a further pH decrease by the hydrolysis reaction. Hence, the pH drop is distinct in case of no addition of nitric acid in which the solid concentration is increased by the rising $c_{\text{reactant.Cu(NO}_3)_2}$.

The variation in pH and solid weight is less pronounced with addition of nitric acid than without addition of nitric acid. The pH decreases from approximately 7 to 5.5. The pH of 5.5 is reached using 0.075 M $c_{\text{reactant.Cu(NO}_3)_2}$ and does not

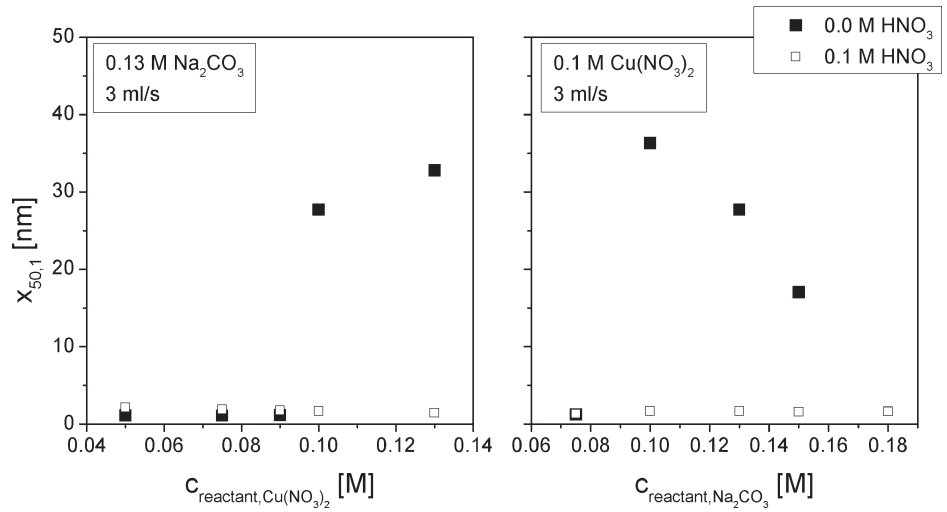

Figure 4. Predicted mean particle sizes $x_{50,1}$ from precipitation simulations with acidified and not acidified $Cu(NO_3)_2$ reactant solution and varying $Cu(NO_3)_2$ (left) and Na_2CO_3 (right) reactant concentration.

change at higher $c_{\text{reactant.Cu(NO}_3)_2}$. At low $c_{\text{reactant.Cu(NO}_3)_2}$ of 0.05 M with addition of nitric or with addition of nitric acid, a solid weight of 0.2 g is obtained. An increase of solid weight from 0.2 g up to 0.4 g is possible adjusting $c_{\text{reactant.Cu(NO}_3)_2}$ to 0.13 M. The increase is half times less in case of addition of nitric acid than without addition of nitric acid.

The pH of simulations is in good agreement with the measured pH at all concentrations $c_{\text{reactant.Cu(NO}_3)_2}$. The pronounced decrease of pH in the experiment by increase of $c_{\text{reactant.Cu(NO}_3)_2}$ is well matched. In case of addition of nitric acid, the pH of simulations reaches a plateau above 0.075 M, which is in agreement with the slight pH change in experiments. At low $c_{\text{reactant.Cu(NO}_3)_2}$ (< 0.1 M), in case of no addition of nitric acid and throughout all $c_{\text{reactant.Cu(NO}_3)_2}$ in case of addition of nitric acid secondary nucleation is considered in the simulations. This leads to a better estimation of the solid weight than without secondary nucleation.

The increase of the sodium carbonate reactant concentration $c_{\text{reactant.Na}_2\text{CO}_3}$ from the reference conditions leads to an experimental pH increase in Figure 7a, from 5.4 to 7.3 without addition of nitric acid and from 5.2 to 6.6 in Figure 7c, with addition of nitric acid. The rise of pH can be explained by the mixing of alkaline sodium carbonate solution into copper nitrate solution. The pH at the ideally mixed state and hence, the pH after solid formation is higher with increasing concentration of sodium carbonate.[13]

In Figure 7d, it can be seen that the solid weight is underestimated using nitric acid and $c_{\text{reactant.Na}_2\text{CO}_3}$ below 0.13 M even if secondary nucleation is used ($\beta_{\text{sec}} = 0.7$) in the simulations. An increase of β_{sec} does not lead to a further increase of solid weight (not shown here). An exception is shown at 0.075 M $c_{\text{reactant.Na}_2\text{CO}_3}$ in Figure 7d. In this case, the solid weight of 4.5×10^{-6} g is increased to 0.066 g by increasing β_{sec} by 0.1 which leads to a better estimation of the solid weight. The activation of secondary nucleation in case of no addition of nitric acid at low $c_{\text{reactant.Na}_2\text{CO}_3}$ (0.075 M) increases the solid weight from 0.016 to 0.32 g, which is in good agreement with measured solid concentration 0.30 g in Figure 7b.

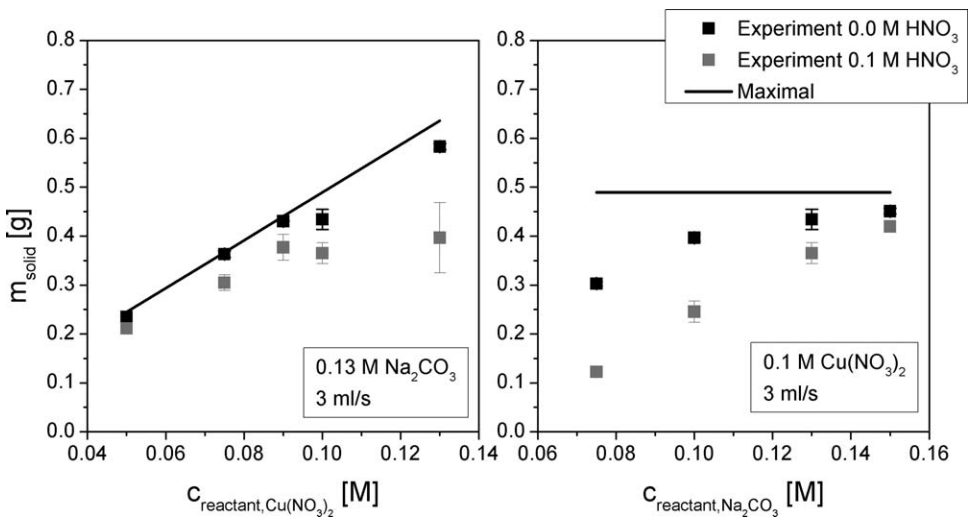

Figure 5. Experimental solid dry weight of precipitates in comparison to the estimation of solid dry weight by assuming maximal consumption of reactants.

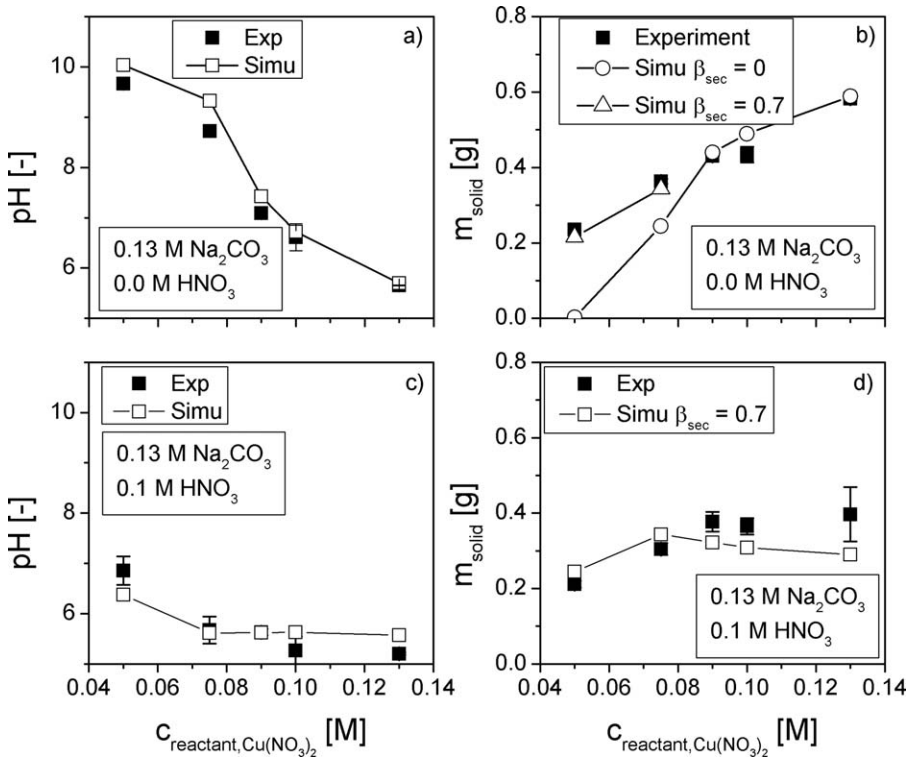

Figure 6. Comparison between measured (Exp) and simulated (Simu) pH of suspension and solid dry weight for acidified and not acidified $Cu(NO_3)_2$ reactant solution and varying $Cu(NO_3)_2$ reactant concentrations.

Hartig et al. showed that secondary nucleation accelerates the solid formation toward shorter time scales.[13] Additionally, an increase of solid concentration, by considering secondary nucleation in simulations, can be seen in Figures 6 and 7. This leads to a better estimation of the solid weight. Low reactant concentrations lead to low supersaturations and to low homogeneous nucleation rates. Secondary nucleation can continue at relatively low values of supersaturation when homogeneous nucleation has almost stopped.[31] The formation of particles by secondary nucleation provides sufficient number concentrations of particles for subsequent growth and hence, solid formation.

The possible sources of errors are discussed in the following. *Ex situ* measurements even with optimized post processing conditions can lead to uncertainties in pH and solid weight. Solid materials can remain on the walls and on the filter membrane after filtration. Hartig et al. showed that most of the carbonate is dissociated as carbonic acid and bicarbonate at the end of simulation.[13] This can lead to a carbon dioxide release during sampling outside the mixing zone which is open to atmosphere. The pH of suspension changes during carbon dioxide release.[25]

Influence of dissociation reactions on solid formation

The solid weight changes without and with nitric acid significantly as shown in Figures 5–7. In case of using nitric acid, the solid weight is always less than without using nitric acid. The influence of nitric acid addition on precipitation is discussed in this section by making use of simulation results at reference conditions.

The temporal evolutions of total concentrations of components and solid concentration during mixing and precipitation at reference conditions without and with addition of nitric acid are shown in Figure 8.

At reference conditions, the mixing zone is filled with 0.13 M sodium carbonate reactant solution and is mixed with 0.1 M copper nitrate solution from outside of the mixing zone. Hence, the total concentration of copper increases, whereas the total concentration of carbonate decreases. The engulfment of copper nitrate reactant solution leads to a dilution of sodium carbonate in the mixing zone. The Georgeite formation is not mixing controlled in the specific power input range of the T-mixer.[13] Mixing and precipitation are decoupled. Hence, the ideally mixed state is reached before particle formation occurs. At the ideally mixed state, which is reached approximately at 3×10^{-3} s at a flow rate of 3 mL/s, the total concentrations of components converge to the half of the reactant concentrations ($c_{\mathrm{tot},CO_3^{2-}} = 0.13\ \mathrm{M}/2$, $c_{\mathrm{tot},Cu^{2+}} = 0.1\ \mathrm{M}/2$). In case of addition of nitric acid, the total nitrate concentration at the ideally mixed state is higher than in case without addition of nitric acid by the nitrate source of HNO_3. The total proton concentration in Figure 8 right is increased already during mixing by engulfment of nitric acid into the mixing zone. A further increase of total proton concentration is caused by hydrolysis reaction of Georgeite precipitation. The total copper and carbonate concentration is decreased by Georgeite formation. In case of addition of nitric acid, solid formation starts immediately when the ideal mixed state is reached indicated by the temporal evolution of solid concentration in Figure 8 right. Georgeite formation without addition of nitric acid in Figure 8 left starts at later time scales. In contrast to the precipitation without addition of nitric acid, the total copper concentration at the end of precipitation with addition of nitric acid is not completely consumed by Georgeite formation.

The total concentrations, shown in Figure 8, are distributed in species concentrations which can be calculated by Eq. 2. By extended Debye–Hückel activity correction, the

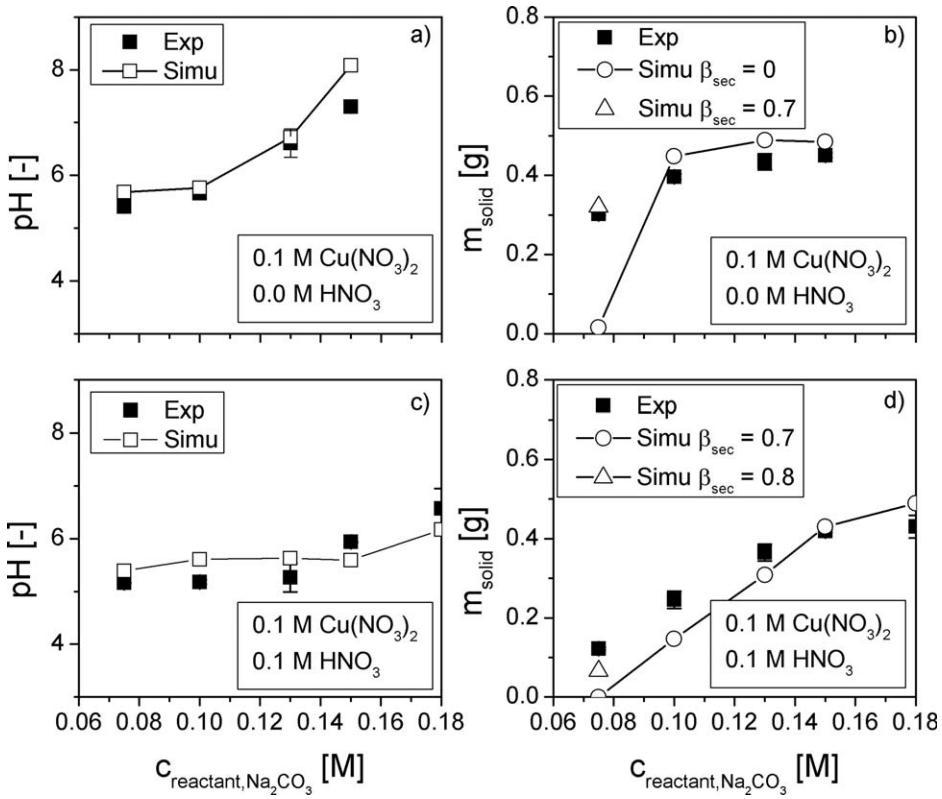

Figure 7. Comparison between measured (Exp) and simulated (Simu) pH of suspension and solid dry weight for acidified and not acidified $Cu(NO_3)_2$ reactant solution and varying Na_2CO_3 reactant concentration.

activities are calculated from the species concentrations.[24] The temporal evolutions of relevant species' activities with and without addition of nitric acid are shown in Figure 9. The temporal evolutions during precipitation in Figure 9 right are plotted between 10^{-4} and 10^{-2} s for the purpose of visibility.

The supersaturation is calculated from the activities of free ions and the solubility product ($S_{Georgeite} = a^2_{Cu^{2+}} \cdot a_{CO_3^{2-}} \cdot a^2_{OH^-} / K_{SP,Georgeite})^{1/5}$. The comparison between left and right side of Figure 9 shows that the addition of nitric acid changes the temporal evolution of species' activities completely and hence, the supersaturation of Georgeite. In the beginning of mixing, both cases start with a high activity of free carbonate and low activity of free copper. By mixing the free carbonate and free copper, activities reach almost the same value and stay at as plateau from 3×10^{-3} s to almost 10^{-1} s leading to a high supersaturation. The supersaturation is much lower in case of addition of nitric acid. The high acidity by addition of nitric acid leads to a lower activity of free carbonate. Instead, carbonate dissociates as $H_2CO_3(aq)$, $CO_2(aq)$, and HCO_3^-. The supersaturation declines by solid formation and reaches a plateau of

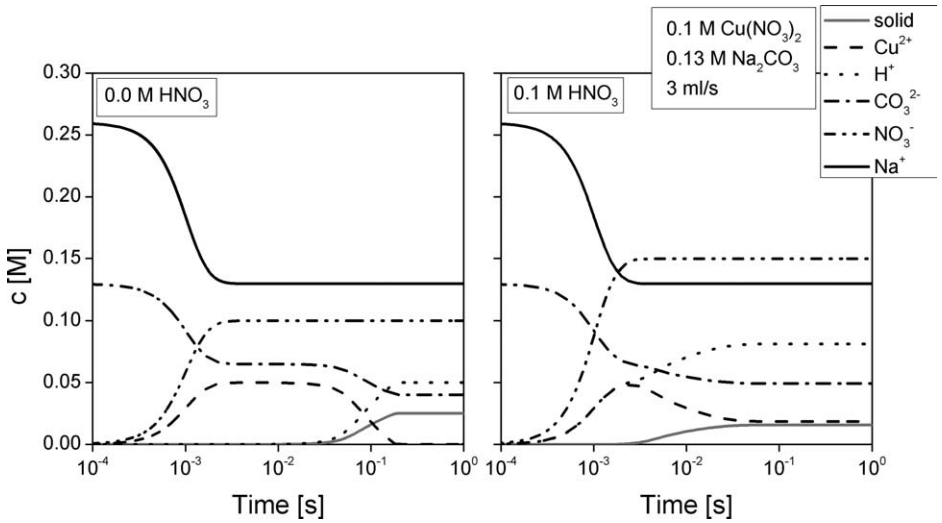

Figure 8. Temporal evolution of total concentrations of components during mixing and precipitation at reference conditions; Left: not acidified $Cu(NO_3)_2$ reactant solution; Right: acidified $Cu(NO_3)_2$ reactant solution.

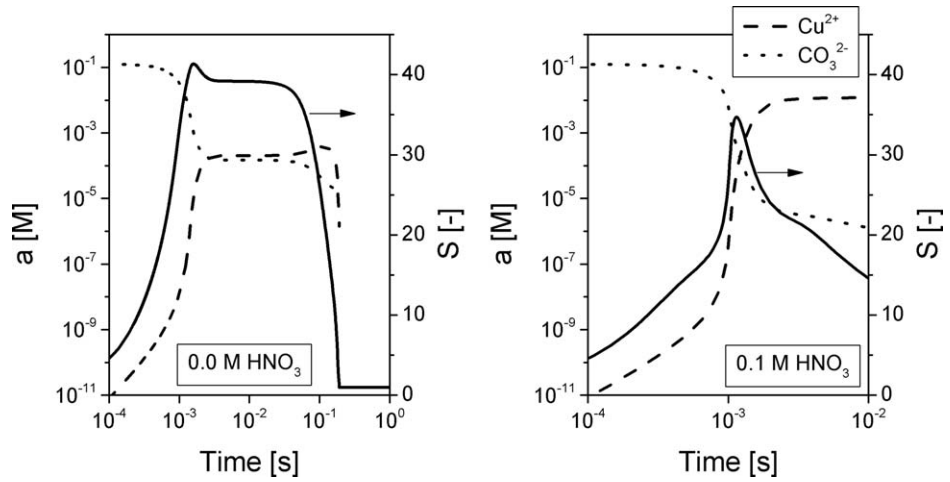

Figure 9. Temporal evolution during mixing and precipitation of free copper and free carbonate activities and supersaturation at reference conditions; Left: not acidified $Cu(NO_3)_2$ reactant solution; Right: acidified $Cu(NO_3)_2$ reactant solution.

approximately $S_{\text{Georgeite}} = 10$. This is in contrast to the precipitation without addition of nitric acid in which the saturated state ($S_{\text{Georgeite}} = 1$) is reached.

In Figure 9, it can be seen that the dissociation of total components' concentrations in species activities determines the supersaturation and hence, the kinetic rates of particle formation in Figure 10.

The long plateau of supersaturation in Figure 9 left leads to a prolonged maximum rate of homogenous nucleation in Figure 10 left. The growth rate reaches immediately a maximum of about 1.5×10^{-6} m/s and stays above 3×10^{-7} m/s for a long time period of approximately 0.05 s. High particle number concentrations are created by homogenous nucleation and grow by diffusion-controlled growth until the solid formation is completed (see solid concentration Figure 8 left). In case of addition of nitric acid, the homogeneous nucleation rate declines after the ideal mixed state is reached. After the first nucleation burst by homogeneous nucleation, the secondary nucleation rate starts to rise and supports the particle formation. The growth rate rises sharply to even higher values as compared to the precipitation without nitric acid addition. However, the growth rate declines fast in the time range where secondary nucleation starts. Both homogeneous and secondary effective nucleation rates stay at approximately $10^2/m^3/s$ from 10^{-1} s at supersaturation level of approximately 10 until the end time of simulation. These rates are too low to complete particle formation in the time scale considered here. This explains the incomplete consumption of the total copper concentration in Figure 8 right. In the experiment, the reaction stops at later time scales during ageing.

Yield of solid formation

The yield of solid formation is a measure, which components from the reactant solutions are consumed by particle formation. It indicates clearly the limitation of solid formation as discussed in Influence of Dissociation Reactions on Solid Formation section. The yield of solid formation in simulation is defined by the ratio of the solid concentration from simulation $c_{\text{solid}}(t = t_{\text{end}})$ and the total component's concentration $c_{\text{tot,p}}(t = 0)$ from reactant solution

$$Y_{p,\text{simu}} = \frac{c_{\text{solid}}(t = t_{\text{end}}) \cdot \beta_p}{c_{\text{tot},p}(t = 0)/2} \times 100\ (\%) \tag{10}$$

$c_{\text{tot},p}(t = 0)$ is corrected as in Eq. 8, by the factor of two because of dilution of reactant solutions by mixing. β_p is used to consider the stoichiometry of the solid in terms of components. The yield of solid formation in experiment $Y_{p,\text{exp}}$ is calculated by the ratio of the solid concentration from experiment by the total component's concentration $c_{\text{tot},p}(t = 0)$ from reactant solution

$$Y_{p,\text{exp}} = \underbrace{\frac{m_{\text{solid,exp}}}{M_{\text{solid}} \cdot V_{\text{reactor}}}}_{c_{\text{solid,exp}}} \cdot \beta_p \cdot \left(c_{\text{tot},p}(t = 0)/2\right)^{-1} \times 100\ (\%) \tag{11}$$

The solid concentration in the experiment is calculated by the molar mass of the solid and the reactor volume based on Eq. 9. The total component's concentration is corrected as in Eq. 10.

The $Cu(NO_3)_2$ reactant concentration and Na_2CO_3 reactant concentration is varied from the reference conditions in experiments and simulation. The yield of solid formation of copper and carbonate components from experiment and simulation is summarized in Figure 11. The yield is shown for using an acidified (Figures 11c and d) and not acidified (Figures 11a and b) $Cu(NO_3)_2$ reactant solution for preparation.

Results from simulation follow the trend of the experimental yield of solid formation qualitatively and even partly quantitatively. Deviations can be seen for low reactant concentrations for the yield of copper component. The yield of carbonate lies always below the yield of copper. One goal in the process of methanol catalyst preparation is to maximize the yield of copper because copper nitrate is the most expensive chemical in the production. Hence, the yield of copper is discussed in the following in detail. In Figure 11b, it can be seen that the yield of copper, in case of precipitation without addition of nitric acid, can be increased from 60% to 100% by increasing the sodium carbonate reactant concentration from 0.075 M toward the reference condition of 0.13 M and above. The variation of copper nitrate reactant

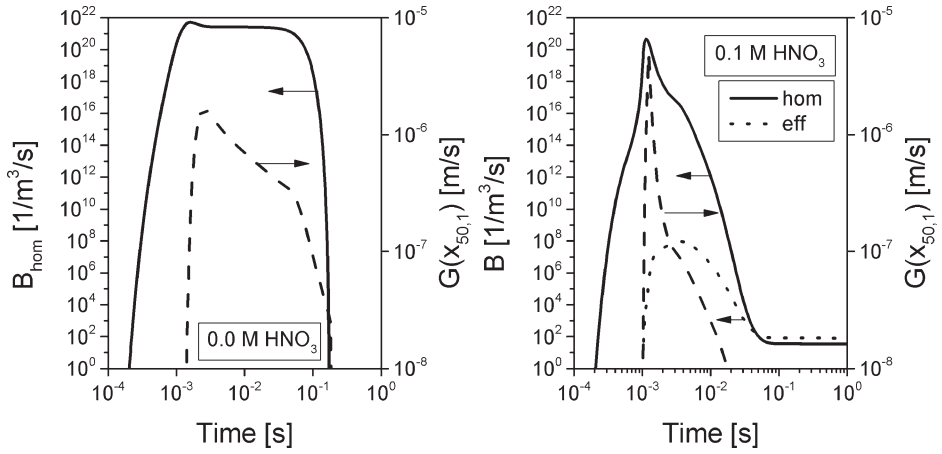

Figure 10. Temporal evolution of nucleation rates and growth rate during mixing and precipitation at reference conditions; Left: not acidified $Cu(NO_3)_2$ reactant solution; Right: acidified $Cu(NO_3)_2$ reactant solution.

concentration using 0.13 M Na_2CO_3 does not influence the yield of copper significantly, which lies already between 80% and 100% (Figure 11a). In case of precipitation with addition of nitric acid, the sodium carbonate reactant concentration plays the major role to gain a high yield of copper. In Figure 11d, it can be seen that the experimental yield of copper can vary in a wide range from 20% to 80% by variation of sodium carbonate reactant concentration from the reference conditions. For a high yield of copper, an over stoichiometric use of sodium carbonate in comparison to copper nitrate is necessary.

Conclusion

The multicomponent and multiphase model of Hartig et al. is applied to the preparation of methanol catalyst precursors in a T-mixer.[13] Reference conditions of catalyst precursor preparation and postprocessing in the T-mixer are chosen in that way that the postprocessing has only minor influence of the characterization of the precipitate.

Georgeite formation is confirmed as favored catalyst precursor phase in a wide range of applied preparation conditions by experimental investigation of the solid phase

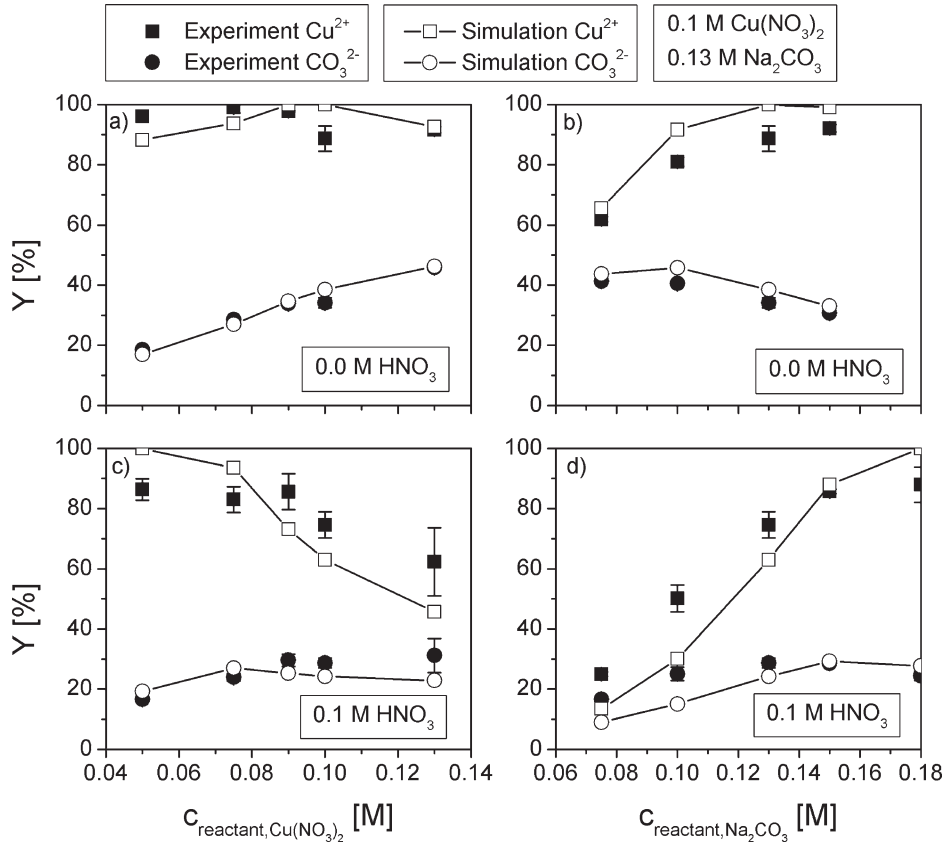

Figure 11. Yield of solid formation of copper and carbonate component from experiment and simulation for acidified and not acidified $Cu(NO_3)_2$ reactant solution for varying $Cu(NO_3)_2$ reactant concentration and varying Na_2CO_3 reactant concentration.

composition of the precipitate. This is in agreement with experiments of Pollard et al. and with our numerical studies.[25] The solid formation at low reactant concentrations can be explained by secondary nucleation. The solid weight is strongly dependent on concentration of the reactant solutions, and a significant change of particle number concentration could be observed with varying reactant concentrations. Two approaches are presented to predict the solid weight of the precipitate. The first approach which is based on the complete consumption of the reactants shows relatively large errors at low sodium carbonate reactant concentrations and high reactant copper nitrate concentrations. The second approach, using simulations based on the model of Hartig et al., leads to significantly reduced errors in a wide range of preparation parameters.[13]

Additionally, it could be shown that for the precipitation of copper catalyst precursors the prediction of the suspension's pH is possible. During precipitation of $Cu/ZnO/Al_2O_3$ methanol synthesis catalysts in stirred vessels, the pH is adjusted by the controlled addition of reactant solutions.[2,27,32] The pH in the initial step has influence on all following steps of the process chain of catalyst production. This effect is denoted as "chemical memory" in literature.[2,10,29,33–36] The pH is seen as a key parameter of catalyst preparation as it affects the phase formation and finally, the specific surface area and productivity of the catalyst.[27,32] Zander et al. could decouple the ageing process from the precipitation to study the ageing independently from other preparation parameters.[8] In this case, the pH could be adjusted by addition of Na_2CO_3 or K_2CO_3 and HNO_3 to the mother liquor. In case of precipitation in a T-mixer, the pH can be controlled by the initial pH of reactant solutions and can now be accessed by simulations within this work. The knowledge of the final chemical composition of the precipitation system from the simulations could improve the control of the pH in the beginning of ageing by addition of further chemicals or buffers.

Furthermore, the yield of copper formation can be controlled by variation of the sodium carbonate reactant concentration and variation of nitric acid concentration in a range between 20% and 100%. Numerical studies show that the reason is the limitation of solid formation by the dissociation of species in aqueous media. This finding can be used to optimize the consumption of copper components by solid formation and to reduce the expenditure of copper salts in the production of copper-based catalysts.

In future, particle size and number concentrations have to be measured to validate additionally disperse properties. This will allow controlling the specific surface area, which is a further key parameter during preparation.[32,37] The network of particles in the SEM image analysis suggest attachment of particles by secondary nucleation or agglomeration. Up to now, the particles are assumed to be separated in our simulations. In future, agglomeration and the balance of the overall agglomerate size have to be considered in our model to estimate and compare the experimental particle sizes to the mean particle sizes of our simulations.

A further focus of future investigations will be the model extension to the zinc, aluminum, or magnesium components toward preparation of commercial $Cu/ZnO/Al_2O_3$ methanol catalysts or alternative copper-based catalysts. For this purpose, the multicomponent and multiphase model was presented here, which is capable to implement various components and solid phases. By this, the model provides a complementary or an even alternative method to study catalyst preparation.

Acknowledgments

The authors would like to thank the German Research Council (DFG) for their financial support of the Cluster of Excellence 'Engineering of Advanced Materials' (www.eam.fau.de) at the University of Erlangen-Nuremberg within the framework of its Excellence Initiative. The authors acknowledge the support of Prof. Karsten Meyer and Dr. Andreas Scheurer for performing the elemental analysis and for fruitful discussions. The authors thank Alexandra Sazonova who helped with precipitation experiments and characterization of precipitates. The authors thank Paula Hoppe who performed ICP-AES measurements.

Literature Cited

1. Deutschmann O, Knözinger H, Kochloefl K, Turek T. Heterogeneous catalysis and solid catalysts, 2. Development and types of solid catalysts. *Ullmann's Encyclopedia Ind Chem.* 2012;17:483–549.
2. Bems B, Schur M, Dassenoy A, Junkes H, Herein D, Schlögl R. Relations between synthesis and microstructural properties of copper/zinc hydroxycarbonates. *Chem Eur J.* 2003;9(9):2039–2052.
3. He L, Cheng H, Liang G, Yu Y, Zhao F. Effect of structure of CuO/ZnO/Al_2O_3 composites on catalytic performance for hydrogenation of fatty acid ester. *Appl Catal A: Gen.* 2013;452:88–93.
4. Hutchings G, Mirzaei A, Joyner R, Siddiqui MR, Taylor S. Ambient temperature CO oxidation using copper manganese oxide catalysts prepared by coprecipitation: effect of ageing on catalyst performance. *Catal Lett.* 1996;42(1–2):21–24.
5. Prieto G, Beijer S, Smith ML, He M, Au Y, Wang Z, Bruce DA, de Jong, Krijn P, Spivey JJ, de Jongh, Petra E. Design and synthesis of copper-cobalt catalysts for the selective conversion of synthesis gas to ethanol and higher alcohols. *Angew Chem Int Ed Engl.* 2014; 53(25):6397–6401.
6. Kundakovic L, Flytzani-Stephanopoulos M. Cu- and Ag-modified cerium oxide catalysts for methane oxidation. *J Catal.* 1998;179(1): 203–221.
7. Li Y, Fu Q, Flytzani-Stephanopoulos M. Low-temperature water-gas shift reaction over Cu- and Ni-loaded cerium oxide catalysts. *Appl Catal B: Environ.* 2000;27(3):179–191.
8. Zander S, Seidlhofer B, Behrens M. In situ EDXRD study of the chemistry of aging of co-precipitated mixed Cu,Zn hydroxycarbonates—consequences for the preparation of Cu/ZnO catalysts. *Dalton Trans.* 2012;41(43):13413–13422.
9. Simson G, Prasetyo E, Reiner S, Hinrichsen O. Continuous precipitation of $Cu/ZnO/Al_2O_3$ catalysts for methanol synthesis in microstructured reactors with alternative precipitating agents. *Appl Catal A: Gen.* 2013;450:1–12.
10. Behrens M, Brennecke D, Girgsdies F, Kissner S, Trunschke A, Nasrudin N, Zakaria S, Idris NF, Hamid SBA, Kniep B, Fischer R, Busser W, Muhler M, Schlögl R. Understanding the complexity of a catalyst synthesis: co-precipitation of mixed Cu, Zn, Al hydroxycarbonate precursors for $Cu/ZnO/Al_2O_3$ catalysts investigated by titration experiments. *Appl Catal A: Gen.* 2011;392(12):93–102.
11. Zander S, Kunkes EL, Schuster ME, Schumann J, Weinberg G, Teschner D, Jacobsen N, Schlögl R, Behrens M. The role of the oxide component in the development of copper composite catalysts for methanol synthesis. *Angew Chem Int Ed.* 2013;52(25):6536–6540.
12. Behrens M, Girgsdies F. Structural effects of Cu/Zn substitution in the malachite-rosasite system. *Z Anorg Allg Chem.* 2010;636(6):919–927.
13. Hartig MAJ, Jacobsen N, Peukert W. Multi-component and multiphase population balance model: the case of Georgeite formation as methanol catalyst precursor phase. *Chem Eng Sci.* 2014;109:158–170.
14. Gradl J. *Experimentelle und theoretische Untersuchungen der Bildungskinetik diffusions- sowie reaktionslimitierter Systeme am Beispiel der Nanopartikelfällung von Bariumsulfat und Zinkoxid.* Dissertation, Göttingen: Cuvillier, 2010.

15. Gradl J, Schwarzer H, Schwertfirm F, Manhart M, Peukert W. Precipitation of nanoparticles in a T-mixer: coupling the particle population dynamics with hydrodynamics through direct numerical simulation. *Chem Eng Process: Process Intensif.* 2006;45(10):908–916.
16. Schur M, Bems B, Dassenoy A, Kassatkine I, Urban J, Wilmes H, Hinrichsen O, Muhler M, Schlögl R. Continuous coprecipitation of catalysts in a micromixer: nanostructured Cu/ZnO composite for the synthesis of methanol. *Angew Chem Int Ed.* 2003;42(32):3815-3817.
17. Kaluza S, Behrens M, Schiefenhövel N, Kniep B, Fischer R, Schlögl R, Muhler M. A novel synthesis route for $Cu/ZnO/Al_2O_3$ catalysts used in methanol synthesis: combining continuous consecutive precipitation with continuous aging of the precipitate. *ChemCatChem.* 2011;3(1):189-199.
18. Schwarzer H, Peukert W. Combined experimental/numerical study on the precipitation of nanoparticles. *AIChE J*. 2004;50(12):3234-3247.
19. Mersmann A. *Crystallization Technology Handbook*, 2nd ed. New York: Marcel Dekker, 2001.
20. Marchisio DL. On the use of bi-variate population balance equations for modelling barium titanate nanoparticle precipitation. *Chem Eng Sci*. 2009;64(4):697–708.
21. Bogacki P, Shampine LF. A 3 (2) pair of Runge-Kutta formulas. *Appl Math Lett*. 1989;2(4):321–325.
22. Morin KA. Simplified explanations and examples of computerized methods for calculating chemical equilibrium in water. *Comput Geosci*. 1985;11(4):409–416.
23. Xu J, Xue D. Fabrication of malachite with a hierarchical sphere-like architecture. *J Phys Chem B*. 2005;109(36):17157–17161.
24. Morel F, Hering JG. *Crystallization Technology Handbook*. New York: Wiley, 1993.
25. Pollard AM, Spencer MS, Thomas RG, Williams PA, Holt J, Jennings JR. Georgeite and azurite as precursors in the preparation of co-precipitated copper/zinc oxide catalysts. *Appl Catal A: Gen.* 1992;85(1):1–11.
26. Shen G, Fujita S, Matsumoto S, Takezawa N. Steam reforming of methanol on binary CuZnO catalysts: effects of preparation condition upon precursors, surface structure and catalytic activity. *J Mol Catal A: Chem.* 1997;124(2–3):123–136.
27. Muhamad EN, Irmawati R, Taufiq-Yap YH, Abdullah AH, Kniep BL, Girgsdies F, Ressler T. Comparative study of Cu/ZnO catalysts derived from different precursors as a function of aging. *Catal Today*. 2008;131(1–4):118–124.
28. Millar GJ, Holm IH, Uwins, Philippa J. R., Drennan J. Characterization of precursors to methanol synthesis catalysts Cu/ZnO system. *Faraday Trans.* 1998;94(4):593–600.
29. Behrens M, Girgsdies F, Trunschke A, Schlögl R. Minerals as model compounds for Cu/ZnO catalyst precursors: structural and thermal properties and IR Spectra of mineral and synthetic (zincian) malachite, rosasite and aurichalcite and a catalyst precursor mixture. *Eur J Inorg Chem.* 2009;2009(10):1347–1357.
30. Schwarzer H. *Nanoparticle Precipitation: An Experimental and Numerical Investigation Including Mixing*. Dissertation, Berlin: Logos-Verlag, 2005.
31. Testino A, Buscaglia V, Buscaglia MT, Viviani M, Nanni P. Kinetic modeling of aqueous and hydrothermal synthesis of barium titanate (BaTiO3). *Chem Mater*. 2005;17(21):5346–5356.
32. Baltes C, Vukojevic S, Schüth F. Correlations between synthesis, precursor, and catalyst structure and activity of a large set of $CuO/ZnO/Al_2O_3$ catalysts for methanol synthesis. *J Catal*. 2008;258(2):334–344.
33. Behrens M. Meso- and nano-structuring of industrial $Cu/ZnO/(Al_2O_3)$ catalysts. *J Catal*. 2009;267(1):24–29.
34. Kasatkin I, Kurr P, Kniep B, Trunschke A, Schlögl R. Role of lattice strain and defects in copper particles on the activity of $Cu/ZnO/Al_2O_3$ catalysts for methanol synthesis. *Angew Chem*. 2007;119(38):7465–7468.
35. Kniep B, Girgsdies F, Ressler T. Effect of precipitate aging on the microstructural characteristics of Cu/ZnO catalysts for methanol steam reforming. *J Catal*. 2005;236(1):34–44.
36. Kurr P, Kasatkin I, Girgsdies F, Trunschke A, Schlögl R, Ressler T. Microstructural characterization of $Cu/ZnO/Al_2O_3$ catalysts for methanol steam reforming—a comparative study. *Appl Catal A: Gen.* 2008;348(2):153–164.
37. Günter MM, Ressler T, Jentoft RE, Bems B. Redox behavior of copper oxide/zinc oxide catalysts in the steam reforming of methanol studied by in situ x-ray diffraction and absorption spectroscopy. *J Catal*. 2001;203(1):133–149.

Manuscript received Nov. 9, 2014, and revision received Feb. 18, 2015.